



UNIVERSITY  
OF WOLLONGONG  
AUSTRALIA

University of Wollongong  
Research Online

---

Faculty of Science, Medicine and Health - Papers

Faculty of Science, Medicine and Health

---

2016

# Rapid Last Glacial Maximum deglaciation in the Indian Himalaya coeval with midlatitude glaciers: new insights from $^{10}\text{Be}$ -dating of ice-polished bedrock surfaces in the Chandra Valley, NW Himalaya

Patricia Eugster  
*University of Potsdam*

Dirk Scherler  
*University of Potsdam*

Rasmus C. Thiede  
*University of Potsdam*

Alexandru Tiberiu Codilean  
*University of Wollongong, codilean@uow.edu.au*

Manfred R. Strecker  
*University of Potsdam*

---

## Publication Details

Eugster, P., Scherler, D., Thiede, R. C., Codilean, A. T. & Strecker, M. R. (2016). Rapid Last Glacial Maximum deglaciation in the Indian Himalaya coeval with midlatitude glaciers: new insights from  $^{10}\text{Be}$ -dating of ice-polished bedrock surfaces in the Chandra Valley, NW Himalaya. *Geophysical Research Letters*, 43 (4), 1589-1597.

Research Online is the open access institutional repository for the University of Wollongong. For further information contact the UOW Library: [research-pubs@uow.edu.au](mailto:research-pubs@uow.edu.au)

---

# Rapid Last Glacial Maximum deglaciation in the Indian Himalaya coeval with midlatitude glaciers: new insights from $^{10}\text{Be}$ -dating of ice-polished bedrock surfaces in the Chandra Valley, NW Himalaya

## **Abstract**

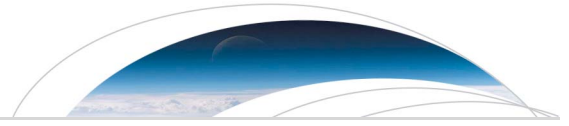
Despite a large number of dated glacial landforms in the Himalaya, the ice extent during the global Last Glacial Maximum (LGM) from 19 to 23 ka is only known to first order. New cosmogenic  $^{10}\text{Be}$  exposure ages from well-preserved glacially polished surfaces, combined with published data, and an improved production rate scaling model allow reconstruction of the LGM ice extent and subsequent deglaciation in the Chandra Valley of NW India. We show that a >1000 m thick valley glacier retreated >150 km within a few thousand years after the onset of LGM deglaciation. By comparing the recession of the Chandra Valley Glacier and other Himalayan glaciers with those of Northern and Southern Hemisphere glaciers, we demonstrate that post-LGM deglaciation was similar and nearly finished prior to the Bølling/Allerød interstadial. Our study supports the view that many Himalayan glaciers advanced during the LGM, likely in response to global variations in temperature.

## **Disciplines**

Medicine and Health Sciences | Social and Behavioral Sciences

## **Publication Details**

Eugster, P., Scherler, D., Thiede, R. C., Codilean, A. T. & Strecker, M. R. (2016). Rapid Last Glacial Maximum deglaciation in the Indian Himalaya coeval with midlatitude glaciers: new insights from  $^{10}\text{Be}$ -dating of ice-polished bedrock surfaces in the Chandra Valley, NW Himalaya. *Geophysical Research Letters*, 43 (4), 1589-1597.



## RESEARCH LETTER

10.1002/2015GL066077

## Key Points:

- Exposure ages of ice-polished surfaces similar to moraine boulders
- Extensive MIS-2 (LGM) glaciation at the southern front of the Indian Himalaya
- Himalayan LGM deglaciation coeval with midlatitude LGM deglaciation

## Supporting Information:

- Text S1, Figures S1–S18, Tables S1 and S2, and Captions for Data Sets S1–S3
- Data Set S1
- Data Set S2
- Data Set S3

## Correspondence to:

P. Eugster,  
eugster@geo.uni-potsdam.de

## Citation:

Eugster, P., D. Scherler, R. C. Thiede, A. T. Codilean, and M. R. Strecker (2016), Rapid Last Glacial Maximum deglaciation in the Indian Himalaya coeval with midlatitude glaciers: New insights from  $^{10}\text{Be}$ -dating of ice-polished bedrock surfaces in the Chandra Valley, NW Himalaya, *Geophys. Res. Lett.*, *43*, 1589–1597, doi:10.1002/2015GL066077.

Received 4 SEP 2015

Accepted 25 JAN 2016

Accepted article online 28 JAN 2016

Published online 22 FEB 2016

## Rapid Last Glacial Maximum deglaciation in the Indian Himalaya coeval with midlatitude glaciers: New insights from $^{10}\text{Be}$ -dating of ice-polished bedrock surfaces in the Chandra Valley, NW Himalaya

Patricia Eugster<sup>1</sup>, Dirk Scherler<sup>2,3</sup>, Rasmus C. Thiede<sup>1</sup>, Alexandru T. Codilean<sup>2,4</sup>, and Manfred R. Strecker<sup>1</sup>

<sup>1</sup>Institute of Earth and Environmental Science, University of Potsdam, Potsdam, Germany, <sup>2</sup>Earth Surface Geochemistry, German Research Centre for Geosciences GFZ, Potsdam, Germany, <sup>3</sup>Institute of Geological Sciences, Freie University Berlin, Berlin, Germany, <sup>4</sup>Now at School of Earth and Environmental Sciences, University of Wollongong, Wollongong, New South Wales, Australia

**Abstract** Despite a large number of dated glacial landforms in the Himalaya, the ice extent during the global Last Glacial Maximum (LGM) from 19 to 23 ka is only known to first order. New cosmogenic  $^{10}\text{Be}$  exposure ages from well-preserved glacially polished surfaces, combined with published data, and an improved production rate scaling model allow reconstruction of the LGM ice extent and subsequent deglaciation in the Chandra Valley of NW India. We show that a >1000 m thick valley glacier retreated >150 km within a few thousand years after the onset of LGM deglaciation. By comparing the recession of the Chandra Valley Glacier and other Himalayan glaciers with those of Northern and Southern Hemisphere glaciers, we demonstrate that post-LGM deglaciation was similar and nearly finished prior to the Bølling/Allerød interstadial. Our study supports the view that many Himalayan glaciers advanced during the LGM, likely in response to global variations in temperature.

### 1. Introduction

The behavior of glaciers is an important climate proxy for changes in humidity and temperature in high mountain ranges, where other climate archives are generally limited. Because the response time of glaciers to varying climate conditions is on the order of tens to hundreds of years, glacial chronologies based on dated moraines are frequently used to infer paleoclimatic conditions [e.g., Putnam *et al.*, 2010]. In the Himalaya, previous studies suggested strong sensitivity of glaciers to variations in precipitation and thus to orbitally driven monsoon intensity. Additional factors may constitute strong east-west gradients in moisture sources, with western areas being influenced by the midlatitude westerlies [e.g., Benn and Owen, 1998] and Northern Hemisphere climate oscillations [e.g., Dortch *et al.*, 2013; Owen and Dortch, 2014]. However, despite a rich collection of >1800 cosmogenic exposure ages that mostly stem from moraines [Dortch *et al.*, 2013; Murari *et al.*, 2014; Owen and Dortch, 2014], it has proven difficult to unambiguously identify the nature of the climatic controls on glacier fluctuations during the late Quaternary period. For example, robust data on advances of Himalayan glaciers during the global Last Glacial Maximum (LGM), here defined as the time period of maximum global ice volume from 19 to 23 ka during Marine Isotope Stage 2 (MIS2) [Mix *et al.*, 2001; Lisiecki and Raymo, 2005], are limited. This particularly applies to the monsoon-influenced sectors of the Himalaya where early last glacial, late glacial, and early Holocene advances are commonly recognized [e.g., Owen, 2009; Scherler *et al.*, 2010; Murari *et al.*, 2014]. Possible reasons for the conundrum of scarce LGM advances include (1) asynchronous or no glacial advances due to steep climatic gradients [Owen *et al.*, 2005] or hypsometric effects [Pratt-Sitaula *et al.*, 2011]; (2) glacial advance due to the impact of rock avalanches and transient increases in debris cover [e.g., Gardner and Hewitt, 1990; Tovar *et al.*, 2008; Jamieson *et al.*, 2015]; (3) large age uncertainties due to unstable till deposits [Applegate *et al.*, 2009; Heyman *et al.*, 2011]; and (4) lack of adequate calibration sites and variations between scaling schemes [Chevalier *et al.*, 2011; Heyman, 2014]. Although asynchronous glacial advances due to topographic effects or steep climatic gradients may exist, it is not very likely that these effects exclusively occur in the Himalaya; yet, so far, there exists limited evidence from other regions. Rock avalanches could trigger asynchronous glacial advances, but these are likely short-lived, local, and subordinate for large glaciers. In contrast, it is well known that erosion rates in the Himalaya are high [Godard *et al.*, 2014; Olen *et al.*, 2015], which makes erosive degradation of moraines a reasonable explanation.

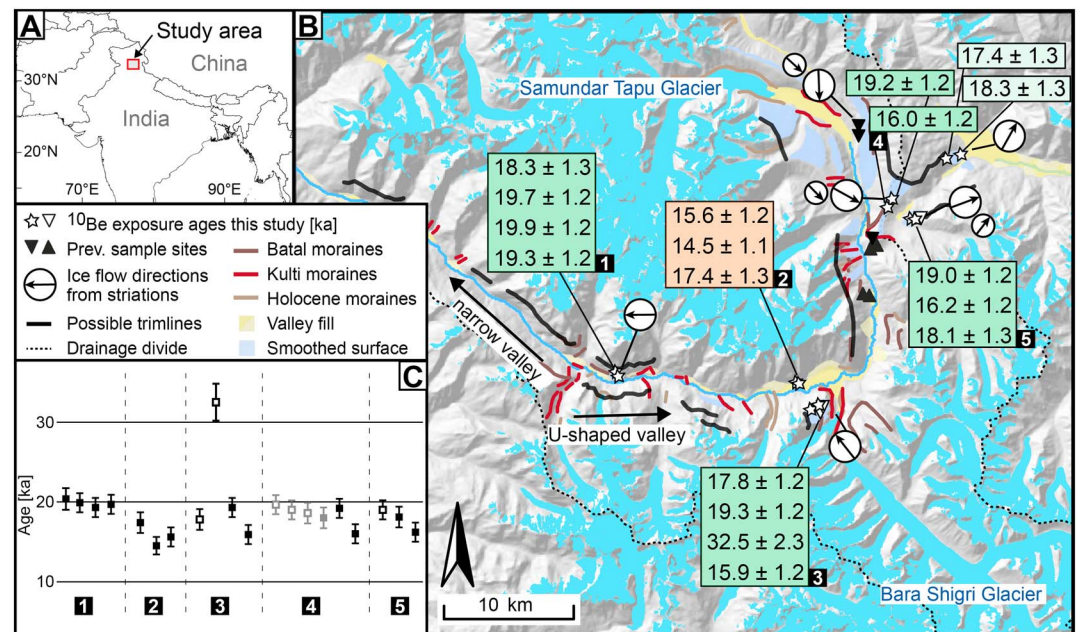


**Figure 1.** Sampling locations and  $^{10}\text{Be}$  exposure ages of this study. (a) Study area. (b) Upper Chandra Valley with mapped landforms, flow directions of glacial striations [Owen *et al.*, 1996, 2001; this study] and modern glaciers [Pfeffer *et al.*, 2014]. White stars and white bottom up triangles indicate sampling locations and corresponding  $^{10}\text{Be}$  exposure ages of this study. Black triangles indicate sampling locations of previous studies [Owen *et al.*, 1996, 2001]. (c) Comparison of  $^{10}\text{Be}$  exposure ages and uncertainties obtained from boulders (white squares) and from glacially polished surfaces black (this study)/grey [Owen *et al.*, 2001]. The numbers correspond to the sampling location in Figure 1b.

Furthermore, there still exist no cosmogenic nuclide calibration sites in the Himalaya, leading to additional methodological age uncertainties. However, recently published new calibrations, including low-latitude and high-altitude sites elsewhere [e.g., Kelly *et al.*, 2013], newly compiled calibration data sets [Heyman, 2014; Borchers *et al.*, 2016], and improved insights into discrepancies between production rate scaling models [Lifton *et al.*, 2014], furnish an improved framework for cosmogenic nuclide exposure dating in the Himalaya.

We revisited the Chandra Valley in the Lahul region, NW Himalaya, where pioneering work by Owen *et al.* [1995, 1996, 1997, 2001] has established the timing of Late Pleistocene glacial advances mainly based on dated boulders. By dating ice-polished, glacially striated bedrock surfaces and reconstructing former ice extents, we are able to refine the existing glacial chronology subsequent to the LGM and suggest that the timing and pace of LGM deglaciation in the Chandra Valley and other Himalayan regions is similar to midlatitude glaciers, and primarily a response to increased global temperatures.

## 2. Study Area

The Chandra Valley, a tributary of the Chenab Valley, lies at  $>3000$  m elevation and is surrounded by peaks higher than 6000 m elevation. The bedrock in the Lahul area comprises Neoproterozoic to Permian granitic intrusions and metasedimentary rocks of the High Himalaya and Tethyan sequences [Steck, 2003]. Among numerous smaller glaciers, the most extensive glaciers in the upper Chandra Valley are Samundar Tapu ( $86\text{ km}^2$ ) [Pfeffer *et al.*, 2014] and Bara Shigri ( $130\text{ km}^2$ ) [Pfeffer *et al.*, 2014] (Figure 1). Trimlines, U-shaped valleys, and dated glacial features attest to a major trunk-valley glaciation, previously referred to as the pre- or syn-LGM Chandra and Batal Glacial stages. The latter stage is manifested by pronounced trimlines and landforms (Batal I) overlain by younger drumlins that indicate readvances (Batal II) along the Chandra and Bhaga Valleys [Owen *et al.*, 1995, 1997, 2001], reassigned to  $15.3 \pm 1.6$  ka [Murari *et al.*, 2014]. Subsequent advances during the Kulti glacial stage are related to tributary glaciers and have been attributed to the Early Holocene [Owen *et al.*, 1995, 1997, 2001] but redefined to the Late Glacial [Murari *et al.*, 2014] and are interpreted as evidence for climatic forcing by the South Asian summer monsoon [Owen *et al.*, 2001] or the midlatitude westerlies [Murari *et al.*, 2014].

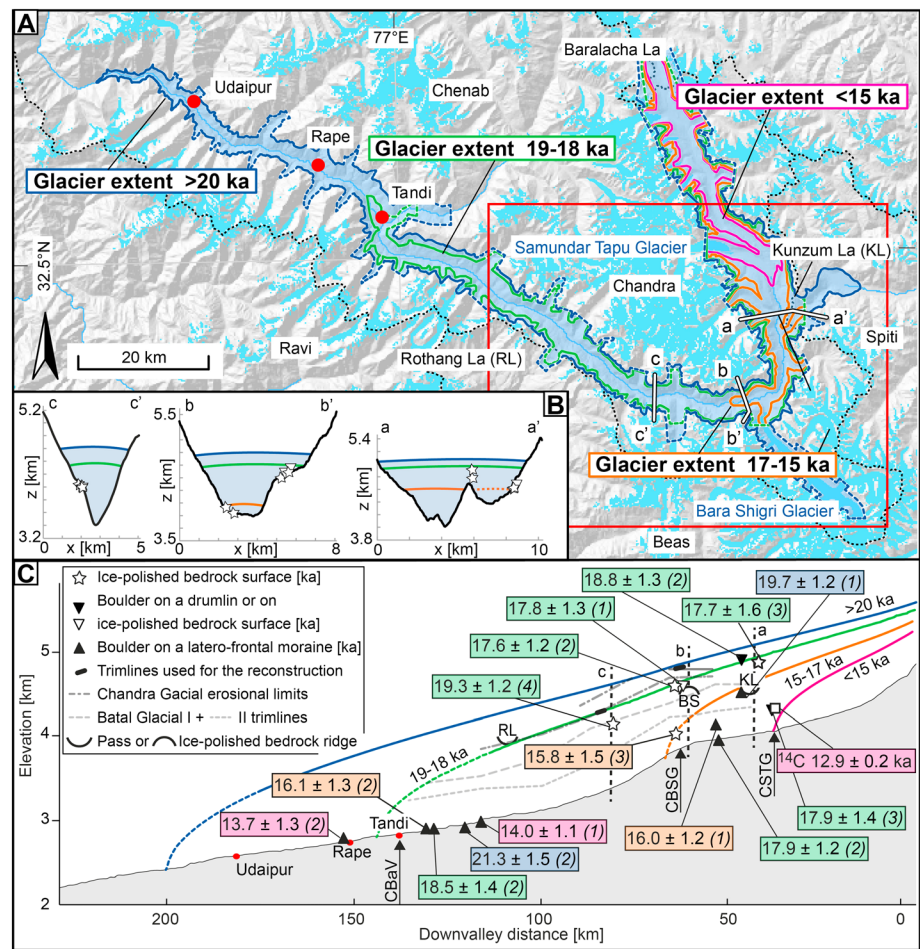


**Figure 2.** Chandra Valley glacier extent during LGM. (a) The Chandra Valley with reconstructed ice extents during the LGM and the subsequent deglaciation. Colors correspond to retreating positions in Figure 2c. White stars and white bottom up triangles indicate our sampling locations. Modern glaciers from Pfeiffer *et al.* [2014] (b) Profiles a-a', b-b', and c-c' show sample locations above the present valley floor. The reconstructed ice thicknesses are shown according to colors in Figure 2c. We included samples from neighboring locations. (c) Retreat history of LGM glacier in the Chandra Valley from Udaipur to the Baralacha La from >20 ka to <15 ka, reconstructed by  $^{10}\text{Be}$  data [Owen *et al.*, 2001; this study] and  $^{14}\text{C}$  data [Rawat *et al.*, 2015]. Mean retreat ages are combined from different studies [Owen *et al.*, 1996, 2001; this study] by the landform they stem from (in parentheses, the number of ages used for the mean age) and are color coded according to the retreating position they belong to. Broken lines in the reconstructions indicate the unclear terminus because of not taking the joining of the Bhaga Glacier and Bara Shigri Glacier into account. Confluence Chandra Valley with main tributary valleys or glaciers indicated by an arrow. CBaV = confluence with Bhaga Valley, CBSG = confluence with Bara Shigri Glacier, CSTG = confluence with Samundar Tapu Glacier.

### 3. Methods

We collected 15 bedrock samples from well-preserved glacially polished surfaces and three samples from boulders resting on these surfaces for cosmogenic  $^{10}\text{Be}$  exposure dating (see supporting information for field photographs and detailed description of sampling locations). After standard mineral separation steps [e.g., Kohl and Nishiizumi, 1992], we extracted Be by ion exchange chromatography at the German Research Centre for Geosciences GFZ in Potsdam.  $^{10}\text{Be}/^9\text{Be}$  ratios were measured by accelerator mass spectroscopy at the University of Cologne [Dewald *et al.*, 2013]. We used the CRONUS-Earth Web Calculator (<http://web1.ittc.ku.edu:8888/1.0/>) hosted at the University of Kansas, which is based on the calibration data set compiled by Borchers *et al.* [2016], for calculating exposure ages for both the new and previously published [Owen *et al.*, 2001]  $^{10}\text{Be}$  concentrations. This calculator uses a new scaling model by Lifton *et al.* [2014] (later also referred to as LSD scaling) that is specific to  $^{10}\text{Be}$  and accounts for its production rate sensitivity on the incident cosmic ray energy spectrum, instead of the cosmic ray flux-based scaling utilized previously. The cosmic ray flux-based scaling schemes do not account for nuclide-specific differences in production rate sensitivities. The CRONUS-Earth Web

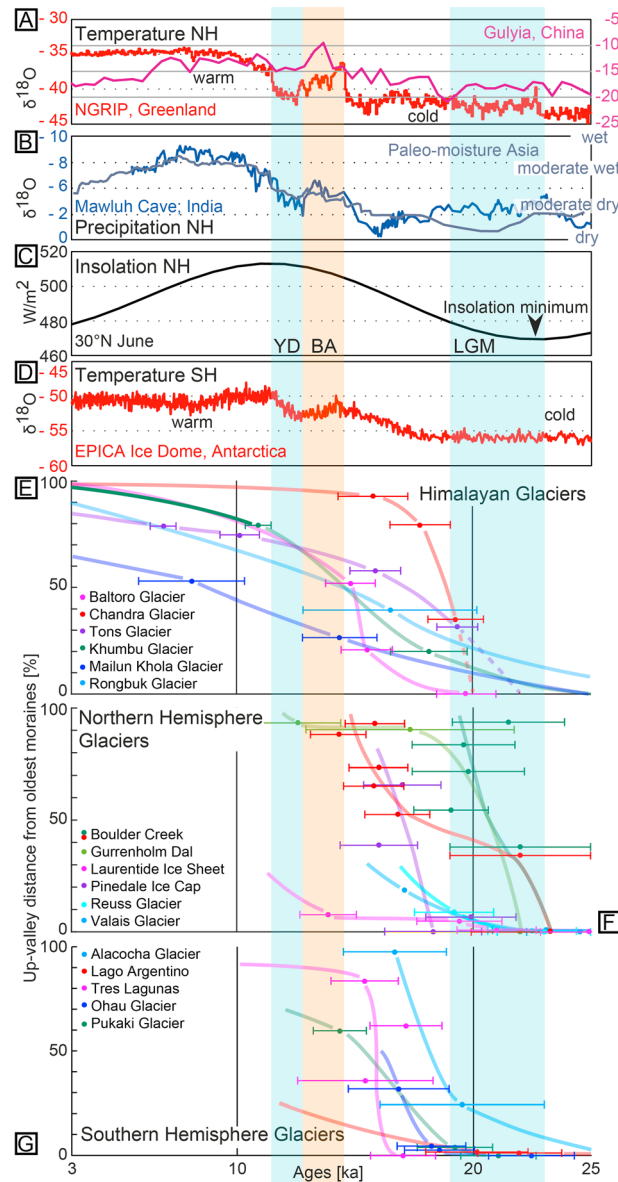


**Figure 3.** Comparison of deglaciation and climate proxies of the Northern and Southern Hemispheres. Glacier retreat indicated as up-valley distance in percent from location of oldest LGM record to the present-day glacier terminus or if vanished to the catchment boundary. Smooth line helps to identify the proposed long-term retreat, in which subtleties of minor glacial advances and retreats may be hidden. Exposure ages on the x axis were recalculated using the CRONUS-Earth Web Calculator hosted at the University of Kansas. YD = Younger Dryas. BA = Bølling/Allerød. (a) NGRIP from Greenland project, Gulyia ice core, (b) Mamwluh Cave  $\delta^{18}\text{O}$  record; effective moisture record (c) Northern insolation; (d) Epica ice dome; (e) Himalayan glacier retreat; (f) Northern Hemisphere glacier retreat; (g) Southern Hemisphere glacier retreat. Full reference list is provided in the supporting information.

neglects tributary glaciers, allowing for the estimation of the ice surface profile of the former trunk glacier, constrained by ice-polished and dated surfaces, moraines, and trimlines. We tested different values of  $\tau_D$  and obtained the best matches with our field constraints using  $\tau_D = 50$  kPa for the maximum ice extent. The longitudinal valley profile and the shape factors (0.4–0.5 in the Chandra Valley) were measured from a

Calculator (hosted by the University of Washington) was also used to recalculate all previously published ages discussed; this information is presented in Figures 1–3 (supporting information provides the references of Figure 3). The reported exposure ages are based on the production rate scaling model by *Lifton et al.* [2014] and a  $^{10}\text{Be}$  half-life of  $1.387 \pm 0.012$  Ma [Chmeleff et al., 2010; Korschinek et al., 2010]. We used the nuclide-specific attenuation lengths described by *Lifton et al.* [2014] with  $145 \text{ g/cm}^2$  for altitudes between 0 and 2 km and  $160 \text{ g/cm}^2$  for  $>3$  km elevations and the thickness correction included in the CRONUS-Earth Web Calculator [Marrero et al., 2016]. In addition, we also calculated all of our ages with the CRONUS online calculator v2.2 using the calibration of *Balco et al.* [2008] and a more extensive calibration data set compiled by *Heyman* [2014].

Topographic shielding was measured in the field with a hand-held compass using the model by *Dunne et al.* [1999]. Snow cover shielding was not accounted for because our sampling sites comprise steep valley flanks and wind-exposed ridges, where thick snow cover is unlikely to remain for long.

We reconstructed the surface profile of the former glacier stepwise from the terminus up-glacier with a simple model that assumes a perfectly plastic ice rheology and a constant driving stress [Benn and Hulton, 2010]:  $h_{i+1} = h_i + (f\tau_D/H)_i(\Delta x/\rho g)$ , where  $h_i$  is the ice surface elevation at node  $i$ ,  $H$  is the ice thickness,  $\tau_D$  is the driving stress,  $\Delta x$  is the node distance,  $\rho$  is the ice density ( $900 \text{ kg/m}^3$ ),  $g$  is acceleration by gravity ( $9.81 \text{ m/s}^2$ ), and  $f$  is a dimensionless shape factor that accounts for valley-side drag and is calculated from  $H$ , the cross-sectional area of the valley  $A$ , and the ice-covered perimeter  $p$ , according to  $f = A/Hp$ . This is a 2-D model that

90 m resolution Shuttle Radar Topography Mission digital elevation model [Jarvis *et al.*, 2008] using MATLAB and the TopoToolbox v2 [Schwanghart and Scherler, 2013].

## 4. Results

### 4.1. Surface Exposure Dating

Our new exposure ages range between ~14 and ~20 ka (Table 1 and Figure 1b). Older ages are obtained from locations with elevations >700 m above the present-day valley floor, while younger ages are obtained from lower elevations. At the Kunzum La (La = pass) (Figure 2b, Profile a-a'), glacial striations indicate that ice was flowing eastward into the Spiti Valley [Owen *et al.*, 1997; Saha *et al.*, 2015], crossing the drainage divide of the Chenab and Sutlej watersheds. Ice-polished bedrock surfaces record ice-free conditions by approximately  $17.6 \pm 1.2$  ka ( $16.0 \pm 1.2$  ka,  $19.2 \pm 1.2$  ka), which is consistent with striations in the upper Spiti Valley dated at  $17.4 \pm 1.3$  and  $18.3 \pm 1.3$  ka. While the previously dated and recalculated surface at the Kunzum La of  $18.0 \pm 1.3$  ka [Owen *et al.*, 2001] is consistent with our data, the boulders dated in that study yield exposure ages of  $19.7 \pm 1.2$  ka,  $19.0 \pm 1.2$  ka, and  $18.6 \pm 1.2$  ka [Owen *et al.*, 1996, 2001], indicating possibly minor inheritance or a readvance. On a bedrock ridge at the Bara Shigri/Chandra confluence (Figure 2b, Profile b-b') at ~4600 m elevation, glacial striations occur ~700 m above the present valley floor on extensive ice-polished surfaces. A trimline at 4800–4900 m elevation separates rugged hillslopes from ice-polished surfaces with a mean age of  $17.6 \pm 2.4$  ka ( $19.3 \pm 1.2$  ka,  $15.9 \pm 1.2$  ka). Two boulders located on this ridge yield ages of  $17.8 \pm 1.3$  ka, consistent with the average surface age, and  $32.5 \pm 2.3$  ka, clearly indicating inheritance. Striated surfaces at lower elevation from the opposite valley side are located 30–150 m above the valley floor and yield a mean age of  $15.8 \pm 1.5$  ka ( $15.6 \pm 1.2$  ka,  $14.5 \pm 1.1$  ka,  $17.4 \pm 1.3$  ka). These results reflect rapid glacier retreat, with the ice thinning by >500 m within ~2 ka. Finally, at a location ~15 km farther downvalley (Figure 2b, Profile c-c'), glacial striations are ~500 m above the valley floor and four samples collected over ~100 m in elevation yield mean exposure ages of  $19.3 \pm 1.2$  ka ( $18.3 \pm 1.3$  ka,  $19.7 \pm 1.2$  ka,  $19.9 \pm 1.2$  ka,  $19.3 \pm 1.2$  ka). We found no more striations farther downstream.

Ages calculated with the CRONUS Earth web calculator using the scaling model by Lifton *et al.* [2014] are generally older than ages calculated with the CRONUS online calculator [Balco *et al.*, 2008] and Heyman's [Heyman, 2014] calibrations. The ages are on average ~25% older comparing Lal/Stone time-dependent ages by Balco *et al.* [2008] and on average ~11% older comparing Lal/Stone time-dependent ages by Heyman [2014] with ages from Lifton *et al.* [2014] for the Himalayan glaciers (see also Table S2 and Figures S17 and S18 in the supporting information).

### 4.2. Glacier Reconstruction and Deglaciation History

Based on the spatial distribution of our new and previously published exposure ages we were able to reconstruct the ice extent in the Chandra Valley between ~20 ka and 15 ka. Our reconstruction suggests that during the LGM, the Chandra Valley was occupied by a glacier up to 1000 m thick (see Figure 2a), which we refer to as the Chandra Valley Glacier or CVG. Both our new ages and reconstruction confirm that glacial ice was crossing major drainage divides such as Kunzum La (~600 m of ice thickness above the present drainage divide) eastward into the Spiti Valley [Saha *et al.*, 2015] and the Rothang La (~400 m ice thickness above the pass) southward into the Beas Valley, also supported by glacial striations [Owen *et al.*, 2001] (Figure 1b). Although no terminal moraines of the former CVG are preserved, likely due to postglacial fluvial erosion in the narrow and deeply incised Chenab Valley, there is evidence that the glacier reached at least the village of Rape [Owen *et al.*, 1997]. Our reconstruction of the ice surface suggests that the glacier extended even beyond Udaipur, reaching a length of ~200 km. However, our reconstruction does not take into account the joining of the Bhaga arm (>100 km) [Owen *et al.*, 1997, 2001] into the trunk valley glacier, which may have resulted in an even longer CVG.

Prior to 19–18 ka, the ice still occupied two drainage divides, but rapid melting had started (Figure 2). Between 17 and 15 ka, the trunk-valley glacier had retreated to a length of ~70 km. After 15 ka, the main trunk valley must have been mostly ice-free, as organic sediments and peat started accumulating near Chandra Lake at  $12.9 \pm 0.2$  ka (radiocarbon age of  $11.0 \pm 0.1$  ka) [Owen *et al.*, 1997; Rawat *et al.*, 2015], which is close to the present terminus of the modern Samundar Tapu Glacier. At the Pleistocene-Holocene transition, tributary valley glaciers readvanced at least once into the trunk valley at around 13 ka (recalculated from

**Table 1.** CRN Data of This Study

| Sample Nr. | Name     | Type <sup>a</sup> | Trust <sup>b</sup> | Location |         | Elevation (masl) | Thickness (cm) | Density (g/cm <sup>3</sup> ) | Production Rate            |                                            | Shielding Factor | Denudation (mm/yr) | Sample Weight (g) | Be Carrier (mg) | <sup>10</sup> Be/ <sup>9</sup> Be <sup>e</sup> (× 10 <sup>-15</sup> ) | <sup>10</sup> Be Concentration (atoms (g qz) <sup>-1</sup> ) | Exposure Age <sup>f,h</sup> (ka) |
|------------|----------|-------------------|--------------------|----------|---------|------------------|----------------|------------------------------|----------------------------|--------------------------------------------|------------------|--------------------|-------------------|-----------------|-----------------------------------------------------------------------|--------------------------------------------------------------|----------------------------------|
|            |          |                   |                    | N        | E       |                  |                |                              | Atoms (g qz) <sup>-1</sup> | Spallation <sup>c</sup> Muons <sup>d</sup> |                  |                    |                   |                 |                                                                       |                                                              |                                  |
| 1          | WP051    | pbs               | 1                  | 32.4164  | 77.6308 | 4760             | 1.5            | 2.65                         | 45.806                     | 0.357                                      | 0.9767           | 0                  | 33.2900           | 0.2765          | 1771 ± 57.0                                                           | 9.81E+5 ± 3.30E+4                                            | 16.0 ± 1.2                       |
| 2          | PE13_01  | pbs               | 1                  | 32.4237  | 77.6357 | 4819             | 3              | 2.6                          | 45.685                     | 0.355                                      | 0.9589           | 0                  | 46.1187           | 0.1496          | 5588 ± 174.0                                                          | 1.21E+6 ± 3.94E+4                                            | 19.2 ± 1.2                       |
| 3          | PE12_013 | pbs               | 0                  | 32.2808  | 77.5779 | 4485             | 3              | 2.65                         | 37.271                     | 0.300                                      | 0.9215           | 0                  | 40.0977           | 0.3063          | 1545 ± 48.2                                                           | 7.88E+5 ± 2.57E+4                                            | 15.9 ± 1.2                       |
| 4          | WP058    | pbs               | 1                  | 32.2822  | 77.5688 | 4491             | 4              | 2.8                          | 39.933                     | 0.321                                      | 0.9944           | 0                  | 28.5550           | 0.2666          | 1705 ± 53.2                                                           | 1.06E+6 ± 3.47E+4                                            | 19.3 ± 1.2                       |
| 5          | WP059    | bos               | 1                  | 32.2823  | 77.5693 | 4499             | 3.5            | 2.8                          | 40.258                     | 0.324                                      | 0.9943           | 0                  | 27.9600           | 0.2664          | 3211 ± 98.6                                                           | 2.04E+6 ± 6.56E+4                                            | 32.5 ± 2.3                       |
| 6          | WP057    | bos               | 1                  | 32.2806  | 77.5676 | 4483             | 3.5            | 2.8                          | 39.949                     | 0.322                                      | 0.9944           | 0                  | 26.7800           | 0.2772          | 1387 ± 43.1                                                           | 9.58E+5 ± 3.12E+4                                            | 17.8 ± 1.3                       |
| 7          | WP052    | pbs               | 1                  | 32.2981  | 77.5538 | 3928             | 3.5            | 2.8                          | 27.517                     | 0.238                                      | 0.9048           | 0                  | 28.1550           | 0.2746          | 981 ± 30.8                                                            | 6.38E+5 ± 2.10E+4                                            | 17.4 ± 1.3                       |
| 8          | WP053    | pbs               | 1                  | 32.2991  | 77.5531 | 4028             | 4              | 2.8                          | 30.527                     | 0.260                                      | 0.9575           | 0                  | 26.5150           | 0.2752          | 828.6 ± 26.9                                                          | 5.73E+5 ± 1.94E+4                                            | 14.5 ± 1.1                       |
| 9          | WP054    | pbs               | 1                  | 32.2993  | 77.5534 | 4039             | 2              | 2.8                          | 31.245                     | 0.266                                      | 0.9578           | 0                  | 28.3850           | 0.2752          | 993.2 ± 31.6                                                          | 6.42E+5 ± 2.13E+4                                            | 15.6 ± 1.2                       |
| 10         | PE12_061 | pbs               | 1                  | 32.3086  | 77.4058 | 4095             | 3              | 2.65                         | 31.553                     | 0.267                                      | 0.9460           | 0                  | 40.1750           | 0.3068          | 1521 ± 47.8                                                           | 7.76E+5 ± 2.54E+4                                            | 18.3 ± 1.3                       |
| 11         | PE12_062 | pbs               | 1                  | 32.3066  | 77.4070 | 4011             | 3              | 2.65                         | 30.078                     | 0.257                                      | 0.9416           | 0                  | 40.0993           | 0.3068          | 1615 ± 50.1                                                           | 8.25E+5 ± 2.67E+4                                            | 19.9 ± 1.2                       |
| 12         | PE12_063 | pbs               | 1                  | 32.3051  | 77.4072 | 3955             | 3              | 2.65                         | 29.534                     | 0.254                                      | 0.9520           | 0                  | 40.4024           | 0.3068          | 1531 ± 47.5                                                           | 7.76E+5 ± 2.52E+4                                            | 19.3 ± 1.2                       |
| 13         | PE12_064 | pbs               | 1                  | 32.3083  | 77.4061 | 4072             | 3              | 2.65                         | 31.700                     | 0.269                                      | 0.9617           | 0                  | 40.3521           | 0.3334          | 1554 ± 48.3                                                           | 8.57E+5 ± 2.79E+4                                            | 19.7 ± 1.2                       |
| 14         | PE12_056 | pbs               | 1                  | 32.4092  | 77.6498 | 4597             | 5              | 2.65                         | 41.413                     | 0.328                                      | 0.9815           | 0                  | 40.0345           | 0.3062          | 1984 ± 61.3                                                           | 1.01E+6 ± 3.27E+4                                            | 18.1 ± 1.3                       |
| 15         | PE12_057 | bos               | 1                  | 32.4093  | 77.6515 | 4612             | 3              | 2.65                         | 42.467                     | 0.337                                      | 0.9831           | 0                  | 19.3261           | 0.3072          | 1044 ± 32.9                                                           | 1.11E+6 ± 3.64E+4                                            | 19.0 ± 1.2                       |
| 16         | PE12_058 | pbs               | 1                  | 32.4085  | 77.6523 | 4608             | 3              | 2.65                         | 42.079                     | 0.334                                      | 0.9760           | 0                  | 40.0975           | 0.3070          | 1782 ± 55.2                                                           | 9.11E+5 ± 2.83E+4                                            | 16.2 ± 1.2                       |
| 17         | PE13_02  | pbs               | 1                  | 32.4507  | 77.6801 | 4568             | 4              | 2.6                          | 38.324                     | 0.305                                      | 0.9114           | 0                  | 16.7413           | 0.1519          | 1483 ± 47.9                                                           | 8.98E+5 ± 3.03E+4                                            | 17.4 ± 1.3                       |
| 18         | PE13_03  | pbs               | 1                  | 32.4540  | 77.6936 | 4184             | 4              | 2.6                          | 33.755                     | 0.281                                      | 0.9698           | 0                  | 46.9540           | 0.1512          | 3857 ± 120.0                                                          | 8.29E+5 ± 2.70E+4                                            | 18.3 ± 1.3                       |

<sup>a</sup>pbs = polished bedrock surface, bos = boulder on polished bedrock surface; all the tops were exposed at the surface.

<sup>b</sup>Trust based on the quality of the sample and the possible earlier shielding due to, e.g., till cover. 1 = very good, 0 = good.

<sup>c</sup>Production rate based on Liffon *et al.* [2014] as described in Borchers *et al.* [2016] and Marrero *et al.* [2016].

<sup>d</sup>Production rate calculated as described in Marrero *et al.* [2016] and Phillips *et al.* [2016].

<sup>e</sup>AMS ratios were normalised to 07KNSSTD standard and corrected using full procedural blanks (n = 5) with <sup>10</sup>Be/<sup>9</sup>Be ratios ranging between 0.9 ± 0.4 and 2.5 ± 0.6 × 10<sup>-15</sup>.

<sup>f</sup>Uncertainties are reported in the 1 sigma confidence level.

<sup>g</sup>Propagated uncertainties include error in the blank, carrier mass (1%), and counting statistics.

<sup>h</sup>Propagated error in the model ages include a 6% uncertainty in the production rate of <sup>10</sup>Be and a 4% uncertainty in the <sup>10</sup>Be decay constant.



Owen *et al.* [2001] and Murari *et al.* [2014]), but there exists no evidence of any trunk-valley glacier advance at this time or later. Well-preserved flood deposits in the Chandra River bed resulting from ice dam failure in the Upper Chandra Valley [Coxon *et al.*, 1996; Owen *et al.*, 2001] and preserved Holocene strath terraces [Adams *et al.*, 2009] support this interpretation. Our reconstruction suggests a mean ice retreat rate of  $37 \pm 11$  m per year in the Chandra Valley beginning at the end of the LGM.

## 5. Discussion

Our new field and  $^{10}\text{Be}$  exposure data and the reconstructed ice extent suggest that during the LGM the Chandra Valley and its tributaries were occupied by a  $\sim 200$  km long and  $\sim 1$  km thick glacier, supporting earlier observations by Owen *et al.* [1995, 1997]. Combining field observations of pronounced trimlines that separate ice-polished surfaces below from rugged bedrock ridges and hillslopes above and sample heights of our new  $^{10}\text{Be}$  ages suggest that earlier advances during the last glacial cycle were either similar or not much more extensive than during the LGM. We favor this interpretation, given the excellent preservation of glacially polished surfaces at high elevation since  $\sim 20$  ka. Furthermore, our ice reconstruction and field evidence support significant overtopping ( $>500$  m) into both the Spiti and Beas Valleys [Owen *et al.*, 1995, 1997, 2001; Saha *et al.*, 2015]. Thus, our reconstructed LGM glacier may not have corresponded to the most extensive glaciation during the last glacial cycle. Comparing our new data and earlier work [Owen *et al.*, 1997, 2001] suggests that our reconstructed LGM ice extent is better correlated with the Chandra glacial stage than the Batal trimlines and, as supported by Murari *et al.*'s [2014] reanalysis, shifts the Batal glacial stage toward the LGM. More dedicated work near the identified trimlines is needed to resolve this issue.

Exposure ages of boulders and ice-polished bedrock surfaces from the same locations within the Chandra Valley are in good agreement with each other and show consistent ages between 19 and 16 ka with no systematic bias (Figure 1c). Because horizontal as well as near-vertical polished surfaces at locations 15–20 km apart from each other yield virtually identical ages, we suggest that in our study, cosmogenic nuclide inheritance is an issue for only one sample, a  $\sim 33$  ka boulder situated on a much younger surface. The similar ages between boulders and surfaces also suggest that glacial erosion has been sufficient to reset all surfaces and that postdepositional erosion of boulder surfaces is negligible.

The reconstructed CVG maintained its maximum vertical extent prior to or at 20 ka, during a weakened Indian Summer Monsoon (Figure 3b) [Herzschuh, 2006; Dutt *et al.*, 2015]. After 20 ka, coeval with increasing temperatures, but also increasing monsoonal strength, the CVG rapidly receded. We thus argue that the retreat of the CVG was primarily driven by temperature; although tributary glaciers with shorter response times could still have reacted to changes in precipitation with minor readvances during a general phase of retreat [Scherler *et al.*, 2011]. Such readvances of tributary glaciers are well documented by remnants of moraines and dated boulders on lateral and frontal moraines of the Kulti glacial stage [Owen *et al.*, 2001].

In Figure 3, we compare the pace and timing of deglaciation in the Chandra Valley with other Himalayan/Karakoram glaciers and midlatitude glaciers from the Northern and Southern Hemispheres based on  $^{10}\text{Be}$  and  $^{14}\text{C}$  ages. We emphasize that we focus here on long-term retreat rates, but acknowledge that the long-term retreat of most glaciers was accompanied by smaller advances and retreats during certain time intervals. As such short-term fluctuations are generally difficult to reconstruct, we did not include them in Figure 3. Although there exist several Himalayan glaciers that did not retreat as fast as the Chandra Valley glacier, and large variations in long-term retreat rates are observable in all regions, most of the glaciers started retreating rapidly close to the end of the LGM (see Figure 3). These observations are consistent with modeled equilibrium line altitudes (ELAs) across Central Asia, which suggest that temperature changes during the LGM controlled the onset of deglaciation [Rupper and Koppes, 2010]. Furthermore, retreat of both Northern and Southern Hemisphere glaciers of comparable size occurred at similar rates as in the Chandra Valley. A recent global compilation of glacial chronologies that excludes the Himalaya points toward a close relationship between globally increasing temperatures and rapid deglaciation [Shakun *et al.*, 2015]. Our new data from the Chandra Valley and recalculated ages from other Himalayan glaciers indicate that rapid post-LGM deglaciation is probably not significantly different from deglaciation elsewhere. Glaciers located in the western Himalaya, in westernmost Tibet, and the Karakoram apparently retreated more rapidly compared to glaciers in the central Himalaya, where the influence of the monsoon is stronger [Finkel *et al.*, 2003; Seong *et al.*, 2007, 2009; Owen *et al.*, 2009].

The new scaling scheme by *Lifton et al.* [2014] affects estimated exposure ages significantly. In the Chandra Valley, recalculated LSD ages deviate from the exposure ages obtained from the CRONUS-Earth online calculator (v2.2) [Balco et al., 2008] by 25% and the calibration data set compiled by *Heyman* [2014] by 11%. Within the Himalaya the differences are 24% and 10%, respectively (see also supporting information Data Set S2 and Figures S17 and S18). Differences within the scaling schemes remain at approximately 10%. In contrast to previous scaling models, the LSD scaling model uses analytical approximations to cosmic ray fluxes in the atmosphere and includes an updated geomagnetic and atmospheric framework [Lifton et al., 2014]. Although the lack of calibration sites within the Himalaya does not yet allow testing whether these improvements also result in more precise ages, a better understanding of the discrepancies between previous scaling models and the resulting bias [Lifton et al., 2014] suggests that some of the existing scaling models have deficiencies. In contrast to the Himalaya, however, the maximum increase of published middle- to high-latitude exposure ages in the Northern and Southern Hemispheres is merely 8% and some locations even show decreasing ages of the same order when using the LSD scaling model.

In light of our new observations and age constraints from the Chandra Valley and the older recalculated moraine ages, it is thus possible that many glacial advances, previously considered to be Late Glacial may be coeval with the LGM confirmed by Optically Stimulated Luminescence ages, e.g., in the Everest region [Richards et al., 2000; Owen et al., 2009]. Importantly, glaciation during the LGM and the pace of retreat in the Himalaya appear to have been more akin to midlatitude glaciers than previously thought and thus reflect hemisphere-scale processes rather than close regional links such as monsoonal forcing.

#### Acknowledgments

This research was funded by the graduate school GRK1364 (Shaping Earth's Surface in a Variable Environment) of the German Science Foundation to M.S. and D.S. (DFG, Deutsche Forschungsgemeinschaft, grant STR 373/19-2). R.T. is supported by DFG grant TH 1371/5-1. We are indebted to V. Jain and T. Tsering Longpo for logistical support during our fieldwork in India. We thank T. Schildgen and W. Düsing for help with sample preparation and discussions. We thank N. Lifton and L. Owen for constructive comments that improved the paper. Field photographs and additional information on calculation results are provided in the supporting information of this manuscript.

#### References

- Adams, B., C. Dietsch, L. A. Owen, M. W. Caffee, J. Spotila, and W. C. Haneberg (2009), Exhumation and incision history of the Lahul Himalaya, northern India, based on (U-Th)/He thermochronometry and terrestrial cosmogenic nuclide methods, *Geomorphology*, 107(3–4), 285–299, doi:10.1016/j.geomorph.2008.12.017.
- Applegate, P. J., N. M. Urban, K. Keller, and R. B. Alley (2009), Modeling the statistical distributions of cosmogenic exposure dates from moraines, *Geosci. Model Dev. Discuss.*, 3(1), 293–307, doi:10.5194/gmdd-2-1407-2009-supplement.
- Balco, G., J. O. Stone, N. A. Lifton, and T. J. Dunai (2008), A complete and easily accessible means of calculating surface exposure ages or erosion rates from  $^{10}\text{Be}$  and  $^{26}\text{Al}$  measurements, *Quat. Geochronology*, 3(3), 174–195, doi:10.1016/j.quageo.2007.12.001.
- Benn, D. I., and N. R. J. Hulton (2010), An Excel™ spreadsheet program for reconstructing the surface profile of former mountain glaciers and ice caps, *Comput. Geosci.*, 36(5), 605–610, doi:10.1016/j.cageo.2009.09.016.
- Benn, D. I., and L. A. Owen (1998), The role of the Indian summer monsoon and the mid-latitude westerlies in Himalayan glaciation: Review and speculative discussion, *J. Geol. Soc.*, 155, 353–363, doi:10.1144/gsjgs.155.2.0353.
- Borchers, B., S. Marrero, G. Balco, M. Caffee, B. Goehring, N. Lifton, K. Nishiizumi, F. Phillips, J. Schaefer, and J. Stone (2016), Geological calibration of spallation production rates in the CRONUS-Earth project, *Quat. Geochronology*, 31, 188–198, doi:10.1016/j.quageo.2015.01.009.
- Chevalier, M.-L., G. Hilley, P. Tapponnier, J. Van Der Woerd, J. Liu-Zeng, R. C. Finkel, F. J. Ryerson, H. Li, and X. Liu (2011), Constraints on the late Quaternary glaciations in Tibet from cosmogenic exposure ages of moraine surfaces, *Quat. Sci. Rev.*, 30(5–6), 528–554, doi:10.1016/j.quascirev.2010.11.005.
- Chmeleff, J., F. von Blanckenburg, K. Kossert, and D. Jakob (2010), Determination of the  $^{10}\text{Be}$  half-life by multicollector ICP-MS and liquid scintillation counting, *Nucl. Instrum. Methods Phys. Res., Sect. B*, 268(2), 192–199, doi:10.1016/j.nimb.2009.09.012.
- Coxon, P., L. A. Owen, and W. A. Mitchell (1996), A late Quaternary catastrophic flood in the Lahul Himalayas, *J. Quat. Sci.*, 11(6), 495–510, doi:10.1002/(SICI)1099-1417(199611/12)11:6<495::AID-JQS268>3.0.CO;2-M.
- Dewald, A., et al. (2013), CologneAMS, a dedicated center for accelerator mass spectrometry in Germany, *Nucl. Instrum. Methods Phys. Res., Sect. B*, 294, 18–23, doi:10.1016/j.nimb.2012.04.030.
- Dortch, J. M., L. A. Owen, and M. W. Caffee (2013), Timing and climatic drivers for glaciation across semi-arid western Himalayan–Tibetan orogen, *Quat. Sci. Rev.*, 78, 188–208, doi:10.1016/j.quascirev.2013.07.025.
- Dunne, J., D. Elmore, and P. Muzikar (1999), Scaling factors for the rates of production of cosmogenic nuclides for geometric shielding and attenuation at depth on sloped surfaces, *Geomorphology*, 27(1–2), 3–11, doi:10.1016/S0169-555X(98)00086-5.
- Dutt, S., A. K. Gupta, S. C. Clemens, H. Cheng, R. K. Singh, G. Kathayat, and R. L. Edwards (2015), Abrupt changes in Indian summer monsoon strength during 33,800 to 5500 years B.P., *Geophys. Res. Lett.*, 42, 5526–5532, doi:10.1002/2015GL064015.
- Finkel, R. C., L. A. Owen, P. L. Barnard, and M. W. Caffee (2003), Beryllium-10 dating of Mount Everest moraines indicates a strong monsoon influence and glacial synchronicity throughout the Himalaya, *Geology*, 31(6), 561, doi:10.1130/0091-7613(2003)031<0561:BDOMEM>2.0.CO;2.
- Gardner, J. S., and K. Hewitt (1990), A surge of Bualtar Glacier, Karakoram Range, Pakistan: A possible landslide trigger, *J. Glaciol.*, 36(123), 159–162.
- Godard, V., D. L. Bourlès, F. Spinabella, D. W. Burbank, B. Bookhagen, G. Burch Fisher, A. Moulin, and L. Léanni (2014), Dominance of tectonics over climate in Himalayan denudation, *Geology*, 43(3), 243–246, doi:10.1130/G35342.1.
- Herzschuh, U. (2006), Palaeo-moisture evolution in monsoonal Central Asia during the last 50,000 years, *Quat. Sci. Rev.*, 25(1–2), 163–178, doi:10.1016/j.quascirev.2005.02.006.
- Heyman, J. (2014), Paleoglaciation of the Tibetan Plateau and surrounding mountains based on exposure ages and ELA depression estimates, *Quat. Sci. Rev.*, 91, 30–41, doi:10.1016/j.quascirev.2014.03.018.
- Heyman, J., A. P. Stroeven, J. M. Harbor, and M. W. Caffee (2011), Too young or too old: Evaluating cosmogenic exposure dating based on an analysis of compiled boulder exposure ages, *Earth Planet. Sci. Lett.*, 302(1–2), 71–80, doi:10.1016/j.epsl.2010.11.040.
- Jamieson, S. S. R., M. W. Ewertowski, and D. J. A. Evans (2015), Rapid advance of two mountain glaciers in response to mine-related debris loading, *J. Geophys. Res. Earth Surf.*, 120, 1418–1435, doi:10.1002/2015JF003504.
- Jarvis, A., H. I. Reuter, A. Nelson, and E. Guevara (2008), Hole-filled seamless SRTM data V4, Int. Cent. for Trop. Agric. (CIAT). [Available at <http://srtm.csi.cgiar.org>, Accessed 26 December 2008.]

- Kelly, M. A., T. V. Lowell, P. J. Applegate, F. M. Phillips, J. M. Schaefer, C. A. Smith, H. Kim, K. C. Leonard, and A. M. Hudson (2013), A locally calibrated, late glacial  $^{10}\text{Be}$  production rate from a low-latitude, high-altitude site in the Peruvian Andes, *Quat. Geochronology*, doi:10.1016/j.quageo.2013.10.007.
- Kohl, C. P., and K. Nishiizumi (1992), Chemical isolation of quartz for measurement of in-situ-produced cosmogenic nuclides, *Geochim. Cosmochim. Acta*, 56(9), 3583–3587, doi:10.1016/0016-7037(92)90401-4.
- Korschinek, G., et al. (2010), A new value for the half-life of  $^{10}\text{Be}$  by heavy-ion elastic recoil detection and liquid scintillation counting, *Nucl. Instrum. Methods Phys. Res., Sect. B*, 268(2), 187–191, doi:10.1016/j.nimb.2009.09.020.
- Lifton, N., T. Sato, and T. J. Dunai (2014), Scaling in situ cosmogenic nuclide production rates using analytical approximations to atmospheric cosmic-ray fluxes, *Earth Planet. Sci. Lett.*, 386, 149–160, doi:10.1016/j.epsl.2013.10.052.
- Lisiecki, L. E., and M. E. Raymo (2005), A Pliocene-Pleistocene stack of 57 globally distributed benthic  $\delta^{18}\text{O}$  records, *Paleoceanography*, 20, PA1003, doi:10.1029/2004PA001071.
- Marrero, S. M., F. M. Phillips, B. Borchers, N. Lifton, R. Aumer, and G. Balco (2016), Cosmogenic nuclide systematics and the CRONUScal program, *Quat. Geochronol.*, 31, 160–187, doi:10.1016/j.quageo.2015.09.005.
- Mix, A., E. Bard, and R. Schneider (2001), Environmental processes of the ice age: Land, oceans, glaciers (EPILOG), *Quat. Sci. Rev.*, 20(4), 627–657, doi:10.1016/S0277-3791(00)00145-1.
- Murari, M. K., L. A. Owen, J. M. Dortch, M. W. Caffee, C. Dietsch, M. Fuchs, W. C. Haneberg, M. C. Sharma, and A. Townsend-Small (2014), Timing and climatic drivers for glaciation across monsoon-influenced regions of the Himalayan–Tibetan orogen, *Quat. Sci. Rev.*, 88, 159–182, doi:10.1016/j.quascirev.2014.01.013.
- Olen, S., B. Bookhagen, B. Hoffmann, D. Sachse, D. Adhikari, and M. R. Strecker (2015), Understanding erosion rates at the Himalayan orogenic front: A case study from the Arun Valley, Nepal, *J. Geophys. Res. Earth Surf.*, 120, 2080–2102, doi:10.1002/2014JF003410.
- Owen, L., R. Bailey, E. Rhodes, W. Mitchell, and P. Coxon (1997), Style and timing of glaciation in the Lahul Himalaya, northern India: A framework for reconstructing late Quaternary palaeoclimatic change in the western Himalayas, *J. Quat. Sci.*, 12(2), 83–109.
- Owen, L. A. (2009), Latest Pleistocene and Holocene glacier fluctuations in the Himalaya and Tibet, *Quat. Sci. Rev.*, 28(21–22), 2150–2164, doi:10.1016/j.quascirev.2008.10.020.
- Owen, L. A., and J. M. Dortch (2014), Nature and timing of Quaternary glaciation in the Himalayan–Tibetan orogen, *Quat. Sci. Rev.*, 88, 14–54, doi:10.1016/j.quascirev.2013.11.016.
- Owen, L. A., D. I. Benn, E. Derbyshire, D. J. A. Evans, W. A. Mitchell, D. Thompson, S. Richardson, M. Lloyd, and C. Holden (1995), The geomorphology and landscape evolution of the Lahul Himalaya, Northern India, *Z. Geomorphol.*, 39(2), 145–174.
- Owen, L. A., E. Derbyshire, S. Richardson, D. I. Benn, D. J. A. Evans, and W. A. Mitchell (1996), The Quaternary glacial history of the Lahul Himalaya, northern India, *J. Quat. Sci.*, 11(1), 25–42.
- Owen, L. A., L. Gualtieri, R. C. Finkel, M. W. Caffee, D. I. Benn, and M. C. Sharma (2001), Cosmogenic radionuclide dating of glacial landforms in the Lahul Himalaya, northern India: Defining the timing of Late Quaternary glaciation, *J. Quat. Sci.*, 16(6), 555–563, doi:10.1002/jqs.621.
- Owen, L. A., R. C. Finkel, P. L. Barnard, M. Haizhou, K. Asahi, M. W. Caffee, and E. Derbyshire (2005), Climatic and topographic controls on the style and timing of Late Quaternary glaciation throughout Tibet and the Himalaya defined by  $^{10}\text{Be}$  cosmogenic radionuclide surface exposure dating, *Quat. Sci. Rev.*, 24(12–13), 1391–1411, doi:10.1016/j.quascirev.2004.10.014.
- Owen, L. A., R. Robinson, D. I. Benn, R. C. Finkel, N. K. Davis, C. Yi, J. Putkonen, D. Li, and A. S. Murray (2009), Quaternary glaciation of Mount Everest, *Quat. Sci. Rev.*, 28(15–16), 1412–1433, doi:10.1016/j.quascirev.2009.02.010.
- Pfeffer, W. T., et al. (2014), The Randolph Glacier Inventory: A globally complete inventory of glaciers, *J. Glaciol.*, 60(221), 537–552, doi:10.3189/2014JoG13J176.
- Phillips, F. M., et al. (2016), The CRONUS-Earth Project: A synthesis, *Quat. Geochronol.*, 31, 119–154, doi:10.1016/j.quageo.2015.09.006.
- Pratt-Sitaula, B., D. W. Burbank, A. M. Heimsath, N. F. Humphrey, M. Oskin, and J. Putkonen (2011), Topographic control of asynchronous glacial advances: A case study from Annapurna, Nepal, *Geophys. Res. Lett.*, 38, L24502, doi:10.1029/2011GL049940.
- Putnam, A. E., G. H. Denton, J. M. Schaefer, D. J. A. Barrell, B. G. Andersen, R. C. Finkel, R. Schwartz, A. M. Doughty, M. R. Kaplan, and C. Schlüchter (2010), Glacier advance in southern middle-latitudes during the Antarctic Cold Reversal, *Nat. Geosci.*, 3(10), 700–704, doi:10.1038/ngeo962.
- Rawat, S., A. K. Gupta, S. J. Sangode, P. Srivastava, and H. C. Nainwal (2015), Late Pleistocene–Holocene vegetation and Indian summer monsoon record from the Lahaul, Northwest Himalaya, India, *Quat. Sci. Rev.*, 114, 167–181, doi:10.1016/j.quascirev.2015.01.032.
- Richards, B. W., L. A. Owen, and E. J. Rhodes (2000), Timing of Late Quaternary glaciations in the Himalayas of northern Pakistan, *J. Quat. Sci.*, 15(3), 283–297, doi:10.1002/(SICI)1099-1417(200003)15:3<283::AID-JQS525>3.0.CO;2-X.
- Rupper, S., and M. Koppes (2010), Spatial patterns in Central Asian climate and equilibrium line altitudes, *IOP Conf. Ser.: Earth Environ. Sci.*, 9(1), 012009, doi:10.1088/1755-1315/9/1/012009.
- Saha, S., M. C. Sharma, M. K. Murari, L. A. Owen, and M. W. Caffee (2015), Geomorphology, sedimentology, and minimum exposure ages of streamlined subglacial landforms in the NW Himalaya, India, *Boreas*, doi:10.1111/bor.12153.
- Scherler, D., B. Bookhagen, M. Strecker, F. von Blanckenburg, and D. Rood (2010), Timing and extent of late Quaternary glaciation in the western Himalaya constrained by  $^{10}\text{Be}$  moraine dating in Garhwal, India, *Quat. Sci. Rev.*, 29(7–8), 815–831, doi:10.1016/j.quascirev.2009.11.031.
- Scherler, D., B. Bookhagen, and M. R. Strecker (2011), Hillslope-glacier coupling: The interplay of topography and glacial dynamics in High Asia, *J. Geophys. Res.*, 116, F02019, doi:10.1029/2010JF001751.
- Schwanghart, W., and D. Scherler (2013), Short communication: TopoToolbox 2—An efficient and user-friendly tool for Earth surface sciences, *Earth Surf. Dyn. Discuss.*, 1, 261–275, doi:10.5194/esurf-d-1-261-2013.
- Seong, Y. B., L. A. Owen, M. P. Bishop, A. Bush, P. Clendon, L. Copland, R. Finkel, U. Kamp, and J. F. Shroder Jr. (2007), Quaternary glacial history of the Central Karakoram, *Quat. Sci. Rev.*, 26(25–28), 3384–3405, doi:10.1016/j.quascirev.2007.09.015.
- Seong, Y. B., L. A. Owen, C. Yi, and R. C. Finkel (2009), Quaternary glaciation of Muztag Ata and Kongur Shan: Evidence for glacier response to rapid climate changes throughout the Late Glacial and Holocene in westernmost Tibet, *Geol. Soc. Am. Bull.*, 121(3–4), 348–365, doi:10.1130/B26339.1.
- Shakun, J. D., P. U. Clark, F. He, N. A. Lifton, Z. Liu, and L. Otto-Bliesner (2015), Regional and global forcing of glacier retreat during the last deglaciation, *Nat. Commun.*, 6, 8059, doi:10.1038/ncomms9059.
- Steck, A. (2003), Geology of the NW Indian Himalaya, *Eclogae Geol. Helv.*, 96(2), 147–196, doi:10.1007/s00015-003-1091-4.
- Tovar, D. S., J. Shulmeister, and T. R. Davies (2008), Evidence for a landslide origin of New Zealand’s Waiho Loop moraine, *Nat. Geosci.*, 1(8), 524–526, doi:10.1038/ngeo249.